



Imaging-Based Characterization of Perthite in the Upper Triassic Yanchang Formation Tight Sandstone of the Ordos Basin, China

DU Shuheng^{1,2,*}, SHI Guoxin^{3,4}, YUE Xinjian^{3,4}, KOU Gen^{3,4}, ZHOU Bo^{3,4} and SHI Yongmin⁵

¹ State Key Laboratory of Nonlinear Mechanics, Institute of Mechanics, Chinese Academy of Sciences, Beijing 100190, China

² Key Laboratory of Petroleum Resources Research, Institute of Geology and Geophysics, Chinese Academy of Sciences, Beijing 100029, China

³ Xinjiang Laboratory of Petroleum Reserve in Conglomerate, Karamay 834000, Xinjiang, China

⁴ Research Institute of Experiment and Detection of PetroChina Xinjiang Oilfield Company, Karamay, 834000, Xinjiang, China

⁵ Oil and Gas Institute, Peking University, Beijing 100871, China

Abstract: This work investigated the element distribution of perthite from the Upper Triassic Yanchang Formation tight sandstone in the Ordos Basin of northern China by field emission scanning electron microscopy (FE-SEM) and energy dispersive spectrometer (EDS). FE-SEM results indicate significant differences in the morphology of Na-rich feldspar when K-rich feldspar is the main component of the perthite. EDS results show that different types of perthite have clearly defined differences on different element indexes. Additionally, indexes such as average-weight-K (K-rich)/Na (Na-rich), maximum-weight-K (Na-rich)/Na (Na-rich) and average-atomic-K (K-rich)/Na(Na-rich) might be the most effective ones to identify perthite types. Perthite is divided into six main types, i.e., perthite with thick parallel stripe distribution, with thin parallel stripe distribution, with lumpy stripe distribution, with dendritic stripe distribution, with encircling stripe distribution, and with mixed stripe distribution.

Key words: petrography, perthite, element distribution, EDS, FE-SEM, image processing, Yanchang Formation, Late Triassic, Ordos Basin

Citation: Du et al., 2019. Imaging-Based Characterization of Perthite in the Upper Triassic Yanchang Formation Tight Sandstone of the Ordos Basin, China. *Acta Geologica Sinica* (English Edition), 93(2): 373–385. DOI: 10.1111/1755-6724.13768

1 Introduction

Perthite is an intergrowth of two feldspars: a host grain of potassium-rich alkali feldspar (near K-feldspar, KAlSi_3O_8 in composition) includes exsolved lamellae or irregular intergrowths of sodic alkali feldspar (near albite, $\text{NaAlSi}_3\text{O}_8$ in composition) (Connors et al., 1995; Zou et al., 2012; Wilde, 2011 and 2013). Typically, the host grain is either orthoclase or microcline (Fig. 1).

The intergrowth of the feldspars forms by exsolution due to a grain of alkali feldspar cooling to an intermediate composition between K-feldspar and albite. Complete solid solution between albite and K-feldspar exists at temperatures near 700°C and pressures like those within the crust of the Earth, but a miscibility gap is present at lower temperatures (Alexandre, 2009; Macquaker et al., 2014). If an alkali feldspar grain with an intermediate composition cools slowly enough, K-rich and more Na-rich feldspar domains separate from one another. In the presence of water, this process occurs quickly.

Perthite intergrowths have a wide variety of shapes. For

example, feldspar minerals are widely present as skeleton minerals in tight sandstone reservoirs of the Yanchang Formation in the Ordos Basin, and the shapes of the K-rich and Na-rich feldspars within the perthite are different. However, no classification schemes of the shapes of perthite in tight sandstone exist; neither does a conclusion about the formation mechanism of the various shapes exist. Therefore, developing a more precise understanding of the mechanism of formation is important (Montgomery et al., 2005; Cuney et al., 2013; Macquaker et al., 2014). Additionally, the development of the stripes in perthite remains to be discussed even though a great deal of research work has been done (Kuschke and Tonking, 1971; Salem et al., 2005; Wilde, 2011). At present, the academic circle has not paid enough attention to the developmental characteristics of striped feldspar in tight sandstone.

Earlier studies of the Yanchang Formation were made (see geology below) but the perthite was not analyzed further. This study aims to concentrate on the structure of the perthite. In this study, field emission scanning electron microscopy (FE-SEM) has been used to identify a large

* Corresponding author. E-mail: dushuheng@imech.ac.cn



Fig. 1. An antiperthitic intergrowth of K-feldspar (the veinlets) in the Na-feldspar (this hand specimen has 7 cm length and 3 cm width from Eurico Zimbres in Wikimedia in 2006).

amount of perthite in the tight sandstone with the aim of providing a new classification system through the statistical analysis of those observations. In addition, the energy dispersive spectrometer technique (EDS) has been used with the aim of determining the distribution of elements in each sample.

2 Geologic Setting

The Ordos Basin is located in the western part of the northern China landmass, and the study area is located in the southwestern part of the northern Shanbei slope in the Ordos Basin (Fig. 2). The Upper Triassic Yanchang Formation comprises clastic rocks dominated by lacustrine sediments formed in the Late Triassic. The physical properties are poor; the average porosity is 8.85%; and the permeability is $0.16 \times 10^{-3} \mu\text{m}^2$ (Wang Zhentao et al., 2015; Sun Jiaopeng et al., 2018). The pore types are mainly intergranular and dissolved pores, and the primary intergranular pore, secondary intergranular pore, and secondary dissolved pore are relatively well-developed (Ma Hongwen et al., 2017; Tan Juanjuan et al., 2017; Sheng Jun et al., 2018; Gao Gang et al., 2018; Liao Jianbo et al., 2018).

Former analyses of rock slices from and XRD of the Yanchang Formation showed that the tight sandstone consisted mainly of various feldspars, quartz, clay minerals, and mica, etc. The feldspars, such as perthite, played the most important role for oil exploration (Xue Chunji, et al., 2011; Tanner et al., 2012; Ao Weihua et al., 2012; Tang Xuan et al., 2012).

3 Methods and Principles

3.1 FE-SEM characterization

FE-SEM is an electronic microscope (instrument model QUANTA-650FEG, produced by FEI) with a high resolution. The instrument can be used for imaging secondary electrons and image processing of the surface morphology of various solid samples (Jarvie et al., 2007; Vengosha et al., 2013; Xin et al., 2015; Huang et al.,

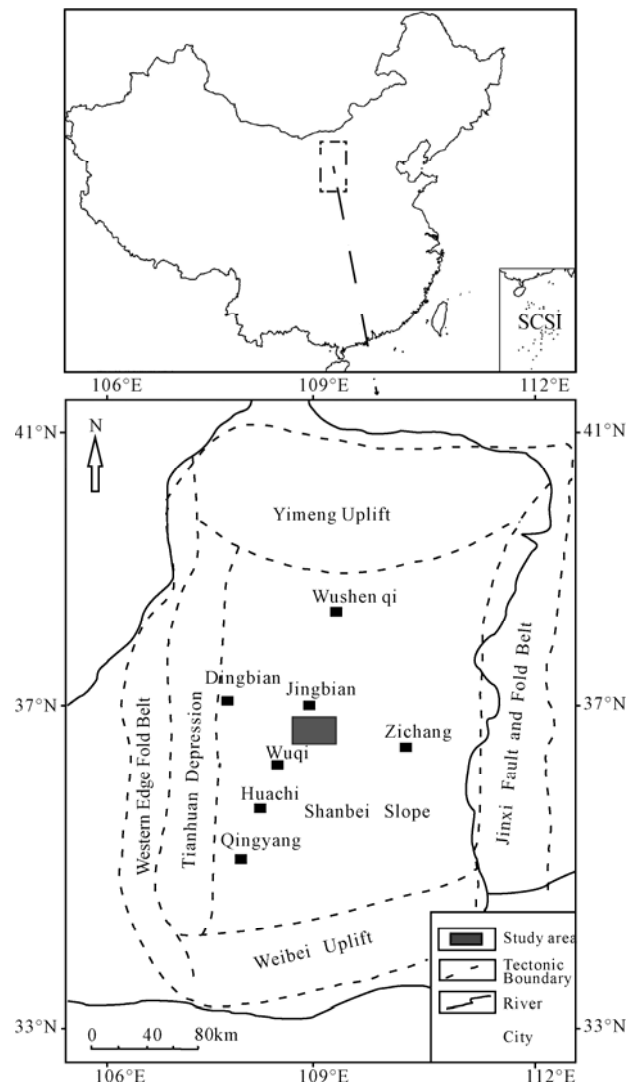


Fig. 2. Location of the study area in the Ordos Basin, China (China basemap after China National Bureau of Surveying and Mapping Geographical Information).

2017). As seen in the imaging of secondary electrons, the instrument can observe samples at low voltage on the basis of coating or no coating to obtain original morphology and ultrastructural information of a sample surface (Fig. 3).

3.2 EDS analysis

The trace element spectrometer (instrument model Inca synergy, produced by Oxford Instruments) can simultaneously perform qualitative, semi-quantitative, and quantitative analysis on the surface of a sample, along with comprehensive analysis of topography and chemical composition (Fig. 4). The EDS technique is one of the most effective methods to determine rock mineral elements and compositions. By detecting mineral elements, the species of minerals can be determined. The determination principle states that different elements have different X-ray photon characteristics. The instrument carries out the analysis of the components through this variation of X-ray photon characteristics (Ding, 1994; Wu



Fig. 3. Thermal field emission scanning electron microscope (Peking University).



Fig. 4. Energy dispersive spectrometer (Peking University).

et al., 2011; Dai et al., 2015).

WDS (spectrograph) and the energy spectrum analysis (using an energy spectrum analyzer) have advantages and disadvantages (Novembre et al., 2005; Mezni et al., 2011; Wang et al., 2017), as follows: (1) the X-ray detection efficiency of the energy spectrometer is high; (2) all elements of the X-ray photons can be measured and

counted at the same time, and the qualitative analysis results can be obtained in a few minutes. The spectrometer can only measure the characteristic wavelengths of each element one by one; (3) the structure is simple, the stability is good, and the reproducibility is good; and (4) the instrument does not need to be concentrated on the surface of the sample and is suitable for rough surface analysis. This is suitable for the characterization of a perthite sample, which may very likely have been exposed to weathering.

The technical process is described in the following flowchart (Fig. 5).

4 Results and Discussion

4.1 FE-SEM characterization

FE-SEM is one of the most effective means to characterize the morphology of rock minerals, because its maximum resolution can reach the nanoscale. A large quantity of perthite was found in the tight sandstone in the Ordos Basin. Eighty-four typical samples were selected as the key objects of this study (Fig. 6).

Figure 6 shows significant differences in the morphology of Na-rich feldspar when K-rich feldspar is the main component of the perthite. SEM characterizations on the perthite in tight sandstone are also shown.

4.2 Perthite classification

According to the differences in morphology, the perthite in sandstone was divided into six main types: perthite with thick parallel stripe distribution, with thin parallel stripe distribution, with lumpy stripe distribution, with dendritic stripe distribution, with encircling stripe distribution, and with mixed stripe distribution, as shown in Table 1. The development probability of the six kinds of stripe feldspar was analyzed, as shown in Fig. 7.

4.3 EDS determination

This study aims to discover why the perthite produced different characteristics, and what differences controlled the morphologies of the perthite. For this purpose, the element content of Na-rich feldspar and K-rich feldspar in

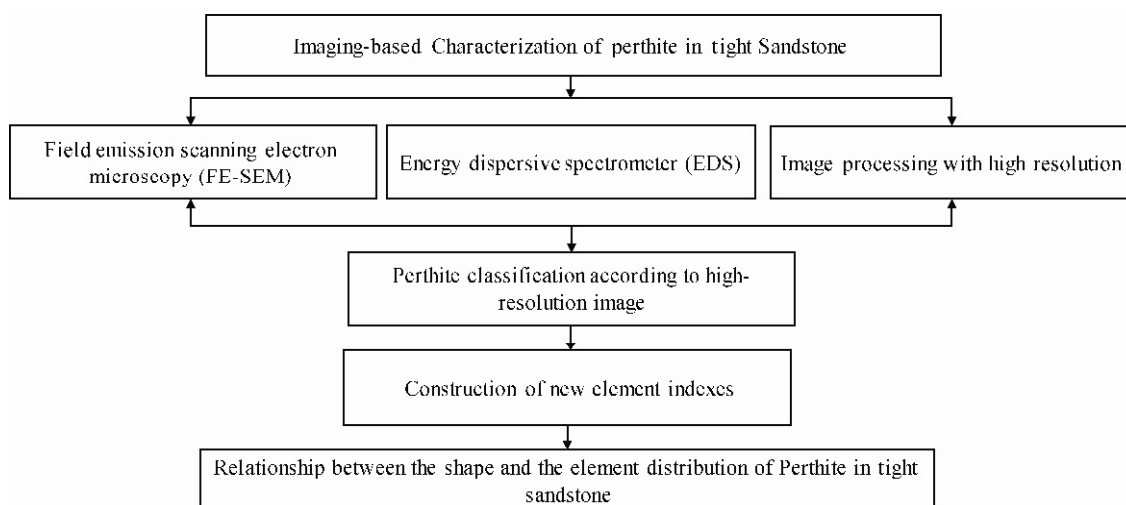


Fig. 5. Technical processes of this study.

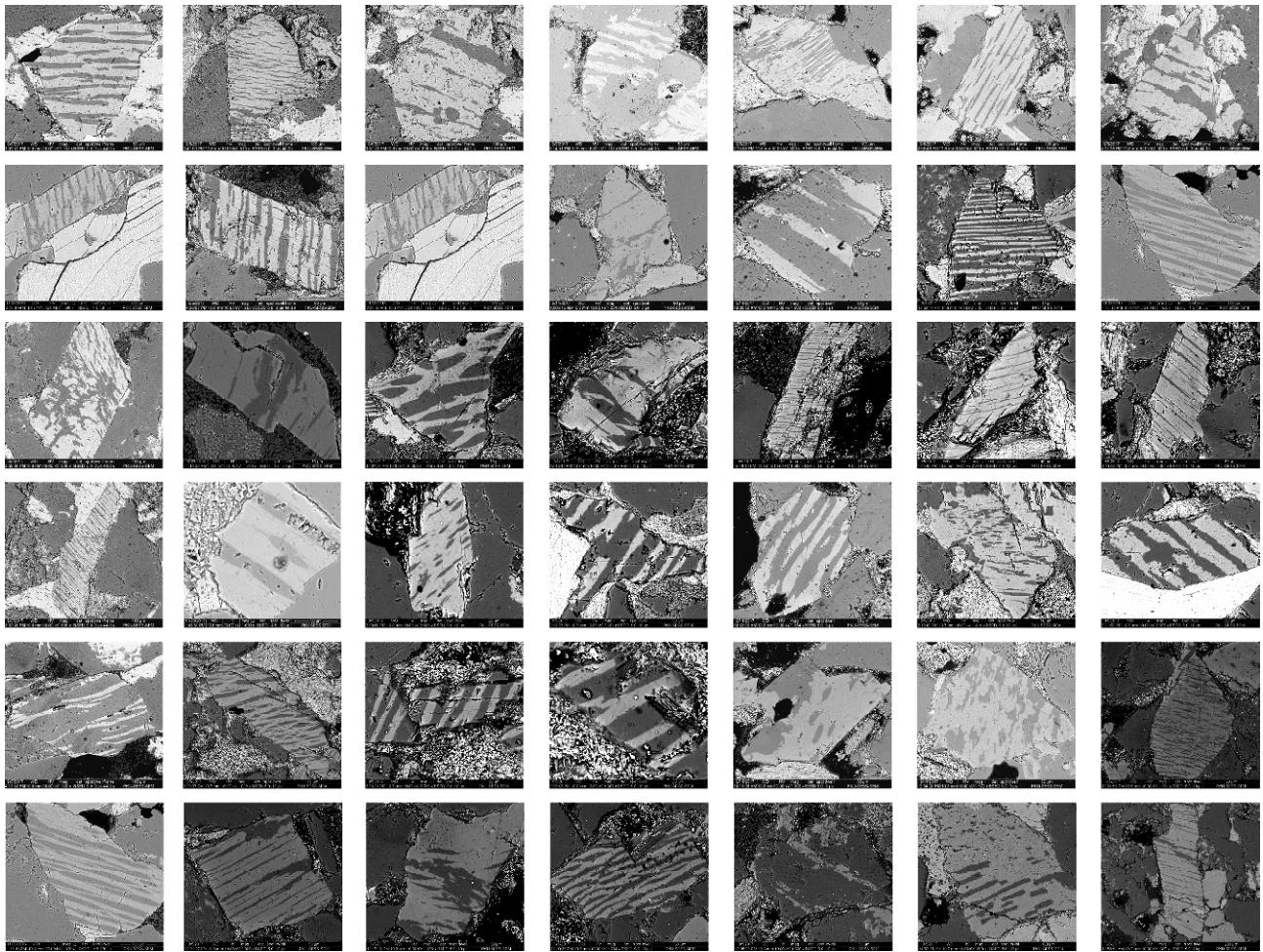


Fig. 6. FE-SEM characterizations on perthite in Upper Triassic tight sandstone, Ordos Basin, China.

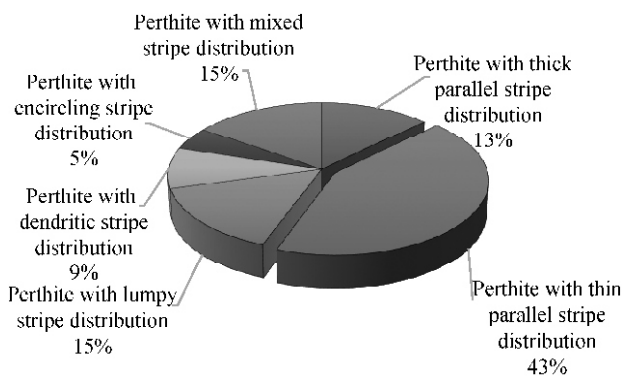


Fig. 7. Statistics of the perthite types in the Upper Triassic tight sandstone.

the perthite were examined and six types discerned, as mentioned above.

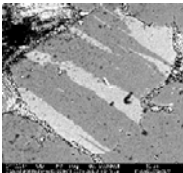
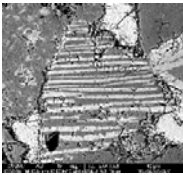
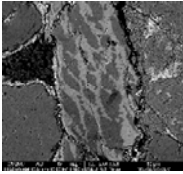
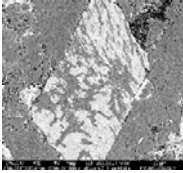
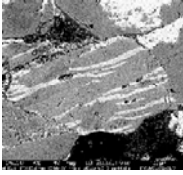
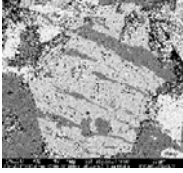
The Na-rich feldspar and K-rich feldspar of 77 samples were determined by elemental analysis, and 154 groups of data were obtained to explore the distribution of the elements in the different shapes of perthite. The EDS analysis results on the perthite in tight sandstone are shown in Fig. 8 and Tables 2–7.

4.4 Construction of new element indexes

As seen in Tables 2–7, the EDS results show that the distribution of elements in the perthite is not uniform, demonstrating that the element analysis results are good indicators of the different perthite samples with various Na-rich feldspar and K-rich feldspar stripes. Based on these results, four new indexes have been constructed. First, the elements K and Na are clearly the most indicative and important for the composition in K-rich feldspar and Na-rich feldspar, respectively. The content ratio of these two elements also indicated the development of the two types of feldspar in the perthite. Second, the Na-rich feldspar in the perthite also sometimes contains the elements K or Ca, or both. However, the discrete content of these two elements might relate to the formation environment. Therefore, the content ratio between K, Ca, and Na might indicate the development of two types of feldspar in the perthite. Third, the K-rich feldspar in the perthite also sometimes contains the element Na; and the content of the element K or Na might also be related to the formation environment. Therefore, the element Na in K-rich feldspar might also indicate the development of two types of feldspar in the perthite.

After constructing the element indexes, the appropriate statistics method was applied to the analysis of all the perthite samples. Making full use of the statistics allowed

Table 1 Classification of the perthite types in the Upper Triassic Yanchang Formation tight sandstone, Ordos Basin, China

Number	Type of perthite	Characteristics description	Typical FE-SEM picture
①	Perthite with thick parallel stripe distribution	The stripe of Na-rich feldspar shows thick parallel line	
②	Perthite with thin parallel stripe distribution	The stripe of Na-rich feldspar shows thin parallel line	
③	Perthite with lumpy stripe distribution	The stripe of Na-rich feldspar shows lumpy individual	
④	Perthite with dendritic stripe distribution	The stripe of Na-rich feldspar shows dendritic lines	
⑤	Perthite with encircling stripe distribution	The stripe of Na-rich feldspar occupied the major part of the perthite	
⑥	Perthite with mixed stripe distribution	The stripe of Na-rich feldspar shows the mixed shape	

for a more accurate conclusion. The average, maximum, minimum, and standard deviations indicated the general level, highest level, lowest level, and the steady state of a set of data, respectively.

The discrete results are as follows: in order to describe the phenomenon and mechanism more conveniently, the six types of perthite were numbered ①, ②, ③, ④, ⑤ and ⑥ to indicate the styles of the tight sandstone perthite as denoted in Table 1.

4.4.1 Average deviation

According to the average deviation, the different types

of perthite had obvious differences in the four element indexes (Figs. 9–10). For K(K-rich)/Na(Na-rich), the level sequences of weight and atomic are ③⑤④②⑥① and ③④⑤②①⑥, respectively; for K(Na-rich)/Na(Na-rich), the level sequences of weight and atomic were ③②④⑥①⑤ and ③②④⑥①⑤, respectively; for Ca(Na-rich)/Na(Na-rich), the level sequences of weight and atomic were ⑤③⑥②④① and ⑤③⑥②④①, respectively; and for Na(K-rich)/K(K-rich), the level sequences of weight and atomic were ①④②⑥③⑤ and ④②⑥①③⑤, respectively.

4.4.2 Maximum deviation

Similarly, according to the maximum deviation, different types of perthite had obvious differences in the four element indexes (Figs. 11–12). For K(K-rich)/Na(Na-rich), the level sequences of weight and atomic were ②③④①⑥⑤ and ②③④①⑥⑤, respectively; for K(Na-rich)/Na(Na-rich), the level sequences of weight and atomic were ②③⑥④①⑤ and ②③⑥④①⑤, respectively; for Ca(Na-rich)/Na(Na-rich), the level sequences of weight and atomic were ②①⑥⑤④③ and ②①⑥⑤④③, respectively; and for Na(K-rich)/K(K-rich), the level sequences of weight and atomic were ①②④⑥③⑤ and ②④⑥③①⑤, respectively.

4.4.3 Minimum deviation

Likewise, according to the minimum deviation, different types of perthite had obvious differences in the indexes (Figs. 13–14). For K(K-rich)/Na(Na-rich), the level sequences of weight and atomic were ⑤④③⑥②① and ⑤④③①⑥②, respectively; for K(Na-rich)/Na(Na-rich), the values of weight and atomic were all equal(0); for Ca(Na-rich)/Na(Na-rich), the values of weight and atomic were all equal(0); and for Na(K-rich)/K(K-rich), the values of weight and atomic were also all equal (0).

4.4.4 Standard deviation

Similarly, according to the standard deviation, different types of perthite had obvious differences in the four element indexes (Figs. 15–16). For K(K-rich)/Na(Na-rich), the level sequences of weight and atomic were ①②③⑥④⑤ and ②③⑥①④⑤, respectively; for K(Na-rich)/Na(Na-rich), the level sequences of weight and atomic were ③②⑥④①⑤ and ③②⑥④①⑤, respectively; for Ca(Na-rich)/Na(Na-rich), the level sequences of weight and atomic were ⑤②①④③⑥ and ⑤②①④③⑥, respectively; and for Na(K-rich)/K(K-rich), the level sequences of weight and atomic were ①②④⑥③⑤ and ②④⑥③①⑤, respectively.

4.4.5 Probability of the occurrence of K and Ca in Na-rich feldspar and K-rich feldspar

Different types of perthite had obvious differences in the four element indexes (Fig. 17). For the probability of the occurrence of K in Na-rich feldspar, the level sequence was ③②④①⑥⑤; for the probability of the occurrence of Ca in Na-rich feldspar, the level sequence was ⑤③⑥②④①; and for the probability of the occurrence of Na in K-rich feldspar, the level sequence was ②⑥④①③⑤.

Table 2 EDS analysis results of perthite with thick parallel stripe distribution

Sample	Percent (%)	Na-rich feldspar						K-rich feldspar						
		C	Na	Al	Si	Ca	K	O	C	Na	Al	Si	K	O
1	Weight	6.46	7.23	7.59	24.43			54.30	4.37		8.20	26.24	1.54	5.83
	Atomic	9.96	5.83	5.21	16.11			62.88	7.22		5.89	18.53	5.34	63.10
2	Weight	4.57	7.62	8.25	26.82			52.74	6.28	0.72	7.59	23.80	8.92	52.68
	Atomic	7.23	6.29	5.80	18.12			62.56	1.50	0.60	5.41	16.28	4.38	63.27
3	Weight	2.13	8.46	8.91	29.91			5.60	3.60	0.49	8.69	26.54	1.74	49.94
	Atomic	3.47	7.21	6.47	2.87			61.98	6.20	0.42	6.46	18.96	5.51	62.62
4	Weight	1.95	6.87	1.52	28.52	1.91		5.22	2.44		8.77	28.52	11.19	49.80
	Atomic	3.22	5.92	7.72	2.10	0.94		62.11	4.15		6.64	2.73	5.84	62.64
5	Weight	4.61	7.35	8.31	26.61		0.49	52.64	3.24	0.59	8.35	27.65	1.28	49.88
	Atomic	7.29	6.80	5.85	18.10		0.24	62.53	5.43	0.52	6.23	19.81	5.29	62.73
6	Weight	1.65	7.55	9.78	29.75	1.17		5.90		0.72	9.79	31.39	11.10	47.00
	Atomic	2.72	6.51	7.18	2.99	0.58		62.20		0.66	7.67	23.62	6.00	62.60
7	Weight	2.91	7.91	8.64	29.14			51.40	2.67	0.52	8.59	28.29	1.60	49.33
	Atomic	4.70	6.67	6.21	2.12			62.30	4.51	0.46	6.46	2.45	5.50	62.61
8	Weight	2.30	8.35	9.21	29.87			5.54	1.99		8.91	28.81	11.82	48.47
	Atomic	3.32	7.13	6.70	2.87			61.99	3.42		6.80	21.13	6.23	62.42
9	Weight	3.30	7.48	8.66	28.72			51.83	2.36		9.40	29.56	9.16	49.88
	Atomic	5.31	6.27	6.19	19.73			62.50	3.98		6.79	21.32	4.75	63.16
10	Weight	2.44	7.96	9.17	29.46			5.98		0.48	9.41	31.54	11.71	46.87
	Atomic	3.96	6.76	6.63	2.47			62.18		0.44	7.39	23.79	6.34	62.50

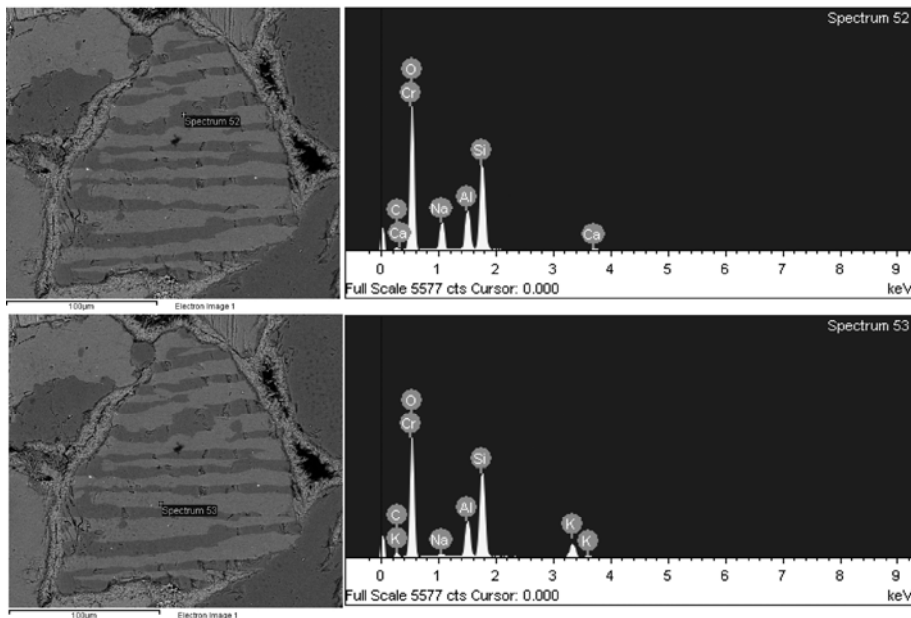


Fig. 8. EDS analysis results of the Na-rich feldspar and K-rich feldspar in perthite in Upper Triassic tight sandstone. Note: the element Cr originates from the conductive coating and does not belong to the mineral.

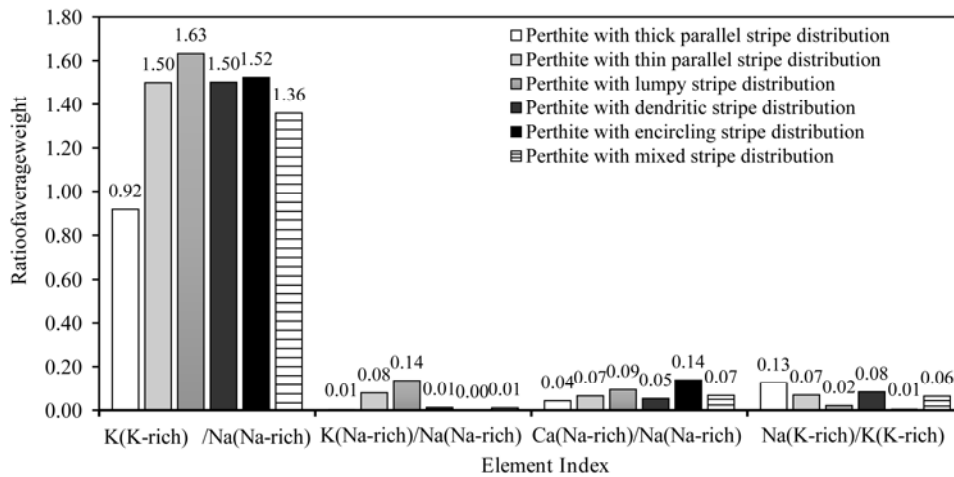


Fig. 9. Ratio of average weight in the perthite in tight sandstone.

Table 3 EDS analysis results of perthite with thin parallel stripe distribution

Sample	Percent (%)	Na-rich feldspar							K-rich feldspar								
		C	Na	Mg	Al	Si	Ca	O	K	Fe	C	Na	Al	Si	K	O	Ba
1	Weight	7.85	6.69		7.22	22.72		55.53			3.68	0.73	8.29	26.38	10.12	49.67	1.14
	Atomic	11.89	5.30		4.87	14.73		63.21			6.18	0.64	6.20	18.95	5.22	62.65	0.17
2	Weight	2.77	2.89	0.37	12.98	26.01		50.68	4.31		3.13		8.45	27.55	11.32	49.55	
	Atomic	4.56	2.48	0.30	9.51	18.31		62.65	2.18		5.27		6.34	19.85	5.86	62.68	
3	Weight	2.35	7.06		9.90	28.22	2.02	50.46			3.38	0.40	8.50	27.05	10.92	49.75	
	Atomic	3.85	6.04		7.22	19.78	0.99	62.11			5.67	0.35	6.34	19.39	5.62	62.62	
4	Weight	2.78	6.51		10.34	27.60	1.77	51.01			2.57	0.66	8.39	28.45	10.79	49.15	
	Atomic	4.53	5.53		7.50	19.22	0.86	62.36			4.35	0.58	6.33	20.61	5.62	62.51	
5	Weight	3.05	7.63		8.94	28.82		51.56			3.95	0.39	7.98	26.83	10.40	50.45	
	Atomic	4.92	6.42		6.41	19.87		62.39			6.55	0.34	5.90	19.05	5.30	62.86	
6	Weight	4.61	7.35		8.31	26.61		52.64	0.49		3.24	0.59	8.35	27.65	10.28	49.88	
	Atomic	7.29	6.08		5.85	18.01		62.53	0.24		5.43	0.52	6.23	19.81	5.29	62.73	
7	Weight	2.31	8.18		9.02	29.66		50.83			2.42	3.19	8.79	28.76	7.23	49.61	
	Atomic	3.77	6.95		6.53	20.65		62.10			4.05	2.79	6.54	20.58	3.72	62.32	
8	Weight	1.78	7.72		10.02	29.28	1.08	50.12			2.43	0.77	8.65	28.68	10.27	49.21	
	Atomic	2.92	6.64		7.34	20.61	0.53	61.94			4.12	0.68	6.52	20.77	5.34	62.57	
9	Weight	2.90	7.90		8.96	28.89		51.36			2.65	0.81	8.22	28.10	11.25	48.97	
	Atomic	4.69	6.66		6.44	19.95		62.26			4.50	0.72	6.20	20.38	5.86	62.34	
10	Weight	2.44	6.79		9.32	28.74	0.96	50.53	1.22		5.44	0.48	7.43	25.09	9.71	51.84	
	Atomic	4.00	5.81		6.80	20.14	0.47	62.16	0.61		8.82	0.41	5.37	17.41	4.84	63.15	
11	Weight	3.86	7.86		8.37	27.79		52.12			4.74	1.59	7.87	25.65	8.92	51.23	
	Atomic	6.16	6.55		5.94	18.95		62.40			7.74	1.36	5.72	17.91	4.48	62.80	
12	Weight	3.86	7.01		9.51	26.26	1.62	51.74			2.69	0.51	8.47	28.23	10.83	49.26	
	Atomic	6.20	5.88		6.79	18.02	0.78	62.34			4.55	0.45	6.38	20.42	5.63	62.56	
13	Weight	3.97	7.50		8.25	27.93		52.35			5.69	0.33	7.45	24.25	10.57	51.70	
	Atomic	6.32	6.24		5.85	19.02		62.57			9.24	0.28	5.39	16.83	5.27	62.99	
14	Weight	4.98	7.29		8.52	26.10		53.11			5.63	0.36	7.68	24.35	10.21	51.77	
	Atomic	7.82	5.99		5.96	17.55		62.68			9.12	0.31	5.55	16.89	5.09	63.05	
15	Weight	2.08	6.96		8.95	29.67		50.16	2.17		2.97		8.52	27.93	11.02	49.57	
	Atomic	3.42	5.99		6.56	20.90		62.03	1.10		5.01		6.40	20.14	5.71	62.75	
16	Weight	2.16	8.01		9.16	29.91		50.76			2.48	0.41	8.48	28.27	11.50	48.86	
	Atomic	3.52	6.82		6.65	20.86		62.15			4.22	0.36	6.43	20.57	6.01	62.41	
17	Weight	2.02	6.80		10.36	28.67	1.81	50.34			1.78	0.79	8.89	29.09	11.12	48.34	
	Atomic	3.32	5.85		7.59	20.17	0.89	62.18			3.05	0.71	6.79	21.34	5.86	62.25	
18	Weight	5.27	7.30		7.73	26.30		53.40			4.19	0.36	8.28	26.00	10.71	50.47	
	Atomic	8.24	5.97		5.39	17.61		62.78			6.95	0.31	6.10	18.42	5.45	62.77	
19	Weight	2.19	7.61		9.27	29.66	0.53	50.74			4.38		7.97	26.14	10.77	50.74	
	Atomic	3.58	6.49		6.74	20.72	0.26	62.21			7.24		5.87	18.47	5.47	62.95	
20	Weight	3.10	7.89		8.80	28.69		51.52			3.34	0.73	8.30	27.53	10.14	49.97	
	Atomic	4.99	6.64		6.31	19.76		62.30			5.58	0.63	6.18	19.68	5.21	62.72	
21	Weight	2.22	8.09		9.23	29.69		50.77			4.70	0.36	8.16	25.83	9.65	51.30	
	Atomic	3.62	6.89		6.69	20.69		62.11			7.70	0.31	5.95	18.09	4.86	63.09	
22	Weight	10.36	5.70		6.85	19.36		57.73			5.65	0.38	7.59	24.65	9.73	52.00	
	Atomic	15.23	4.38		4.49	12.18		63.73			9.14	0.32	5.47	17.06	4.84	63.18	
23	Weight	5.07	6.98		8.40	25.38	1.32	52.85			7.62	0.33	7.16	22.39	8.46	54.03	
	Atomic	8.00	5.76		5.90	17.12	0.62	62.60			11.96	0.27	5.00	15.03	4.08	63.66	
24	Weight	4.07	7.84		8.37	27.44		52.28				0.65	9.55	31.34	11.64	46.81	
	Atomic	6.47	6.51		5.93	18.67		62.42				0.60	7.50	23.63	6.30	61.97	
25	Weight	3.33	8.01		8.67	28.33		51.65				0.54	9.03	31.72	11.91	46.80	
	Atomic	5.35	6.72		6.20	19.45		62.27				0.50	7.10	23.94	6.46	62.01	
26	Weight	2.53	8.42		9.30	28.88		50.86			6.84	1.02	7.25	23.33	8.25	53.30	
	Atomic	4.11	7.14		6.72	20.05		61.98			10.84	0.84	5.11	15.80	4.01	63.38	
27	Weight	4.52	6.92		7.99	27.58		52.98			4.66	0.66	7.74	25.76	10.22	50.96	
	Atomic	7.15	5.72		5.62	18.64		62.87			7.65	0.57	5.66	18.10	5.16	62.86	
28	Weight	2.71	6.84		9.97	27.88	1.70	50.91			2.62	0.38	8.58	28.26	10.98	49.19	
	Atomic	4.41	5.82		7.23	19.43	0.83	62.27			4.44	0.33	6.47	20.48	5.71	62.56	
29	Weight	4.06	7.79		8.07	27.76		52.33			3.79		8.02	27.05	10.86	50.28	
	Atomic	6.45	6.47		5.71	18.88		62.48			6.32		5.95	19.27	5.56	62.89	
30	Weight	5.07	6.89		8.15	26.53		53.37			3.44		8.29	27.29	11.08	49.90	
	Atomic	7.96	5.65		5.69	17.81		62.89			5.77		6.18	19.56	5.70	62.79	
31	Weight	7.85	6.69		7.22	22.72		55.53			3.68	0.73	8.29	26.38	10.12	49.67	1.14
	Atomic	11.89	5.30		4.87	14.73		63.21			6.18	0.64	6.20	18.95	5.22	62.65	0.17
32	Weight	2.98	6.98		9.20	26.99	0.90	52.76	0.18		4.27	2.43	8.44	26.49	7.65	50.72	
	Atomic	4.79	5.87		6.58	18.56	0.44	63.68	0.09		7.00	2.08	6.16	18.56	3.85	62.36	
33	Weight	6.39	6.35		8.51	23.41	1.09	53.98			6.86	0.85	7.29	23.13	8.69	53.19	
	Atomic	9.92	5.15		5.88	15.54	0.51	62.91		0.09	10.89	0.70	5.15	15.69	4.23	63.34	
34	Weight	6.67	4.48		10.46	21.26	0.36	53.65	2.86	0.26	7.03	0.44	7.13	22.88	9.33	53.20	
	Atomic	10.40	3.65		7.27	14.19	0.17	62.86	1.37	0.09	11.16	0.36	5.03	15.53	4.55	63.37	

Table 4 EDS analysis results of perthite with lumpy stripe distribution

Sample	Percent (%)	Na-rich feldspar							K-rich feldspar					
		C	Na	Al	Si	Ca	O	K	C	Na	Al	Si	K	O
1	Weight	2.59	7.27	9.62	28.59	0.99	50.94		3.26		8.58	27.40	10.98	49.78
	Atomic	4.21	6.18	6.97	19.90	0.48	62.25		5.47		6.42	19.68	5.67	62.76
2	Weight	6.58	6.30	8.21	23.53	1.11	54.27		3.23		8.39	27.73	10.78	49.87
	Atomic	10.17	5.09	5.65	15.56	0.52	63.01		5.43		6.27	19.90	5.56	62.84
3	Weight	1.98	7.99	9.11	30.27		50.65			0.86	9.60	31.75	10.61	47.18
	Atomic	3.24	6.83	6.63	21.16		62.15			0.79	7.50	23.83	5.72	62.16
4	Weight	1.74	5.60	9.30	30.07		49.83	3.46			9.35	31.37	12.64	46.64
	Atomic	2.90	4.87	6.88	21.39		62.20	1.77			7.37	23.75	6.87	62.00
5	Weight	3.86	7.08	8.87	27.37	0.71	52.11		4.52		7.80	25.94	10.96	50.78
	Atomic	6.18	5.92	6.31	18.71	0.34	62.54		7.47		5.73	18.31	5.56	62.93
6	Weight	2.09	7.19	10.21	28.58	1.56	50.35		2.33		8.57	28.65	11.60	48.85
	Atomic	3.44	6.17	7.46	20.07	0.77	62.08		3.98		6.51	20.90	6.08	62.54
7	Weight	3.69	4.89	8.70	27.26		51.20	4.26	3.02	0.38	8.33	27.60	11.31	49.35
	Atomic	6.00	4.16	6.29	18.95		62.48	2.13	5.10	0.34	6.26	19.92	5.86	62.52
8	Weight	2.93	7.08	9.84	27.55	1.58	51.03		3.71		8.46	26.93	10.64	50.26
	Atomic	4.75	6.01	7.11	19.14	0.77	62.22		6.18		6.28	19.20	5.45	62.90
9	Weight	3.27	8.26	8.72	28.25		51.51		2.88		8.62	27.92	11.14	49.44
	Atomic	5.25	6.94	6.24	19.42		62.16		4.87		6.49	20.17	5.78	62.70
10	Weight	3.81	7.49	8.85	27.48	0.30	52.06		5.32	0.46	7.77	24.77	10.15	51.54
	Atomic	6.09	6.26	6.29	18.77	0.14	62.44		8.67	0.39	5.63	17.25	5.07	63.00
11	Weight	6.74	6.39	8.26	23.27	0.92	54.41		5.69	0.74	7.52	24.59	9.41	52.05
	Atomic	10.40	5.15	5.67	15.35	0.42	63.01		9.20	0.62	5.41	16.98	4.67	63.12

Table 5 EDS analysis results of perthite with dendritic stripe distribution

Sample	Percent (%)	Na-rich feldspar							K-rich feldspar					
		C	Na	Al	Si	Ca	O	K	C	Na	Al	Si	K	O
1	Weight	2.69	6.82	10.04	27.89	1.67	50.90		2.18	0.87	8.55	28.86	10.76	48.78
	Atomic	4.38	5.81	7.28	19.44	0.81	62.28		3.71	0.77	6.48	21.02	5.63	62.38
2	Weight	4.61	7.52	8.05	27.00		52.82		4.84		7.76	25.63	10.60	51.17
	Atomic	7.28	6.21	5.66	18.23		62.62		7.95		5.67	17.99	5.35	63.05
3	Weight	6.52	7.26	7.32	24.54		54.36			2.03	9.60	31.42	9.88	47.07
	Atomic	10.05	5.84	5.02	16.18		62.91			1.86	7.48	23.52	5.31	61.84
4	Weight	3.05	6.03	6.60	31.89		52.43		3.48	1.57	8.41	27.59	8.47	50.48
	Atomic	4.92	5.07	4.73	21.95		63.35		5.77	1.36	6.21	19.55	4.31	62.80
5	Weight	3.75	7.45	8.68	27.97		52.16		2.27	0.35	8.77	28.40	11.53	48.68
	Atomic	5.99	6.22	6.17	19.10		62.53		3.87	0.31	6.66	20.73	6.05	62.38
6	Weight	10.37	6.18	7.66	23.51	0.46	50.24	0.47	9.18		7.74	24.93	10.56	46.02
	Atomic	15.88	4.94	5.22	15.39	0.21	57.74	0.22	14.93		5.61	17.35	5.28	56.24

Table 6 EDS analysis results of perthite with encircling stripe distribution

Sample	Percent (%)	Na-rich feldspar							K-rich feldspar					
		C	Na	Al	Si	Ca	O	K	C	Na	Al	Si	K	O
1	Weight	1.64	8.07	9.73	29.89	0.56	50.11		2.29		8.82	28.29	11.97	48.63
	Atomic	2.70	6.94	7.13	21.03	0.27	61.92		3.91		6.72	20.68	6.29	62.40
2	Weight	4.80	7.35	8.00	26.83		53.02		3.99		7.93	26.81	10.83	50.44
	Atomic	7.56	6.05	5.61	18.07		62.71		6.62		5.87	19.06	5.53	62.93
3	Weight	2.27	6.84	10.36	28.28	1.72	50.54		2.77	0.40	8.56	28.04	10.92	49.31
	Atomic	3.72	5.86	7.56	19.82	0.84	62.20		4.68	0.35	6.45	20.27	5.67	62.58
4	Weight	2.68	6.83	9.44	26.17	1.59	52.30		7.31		7.88	25.14	10.53	48.04
	Atomic	4.35	5.79	6.82	18.17	0.77	63.73		11.95		5.74	17.59	5.29	59.01

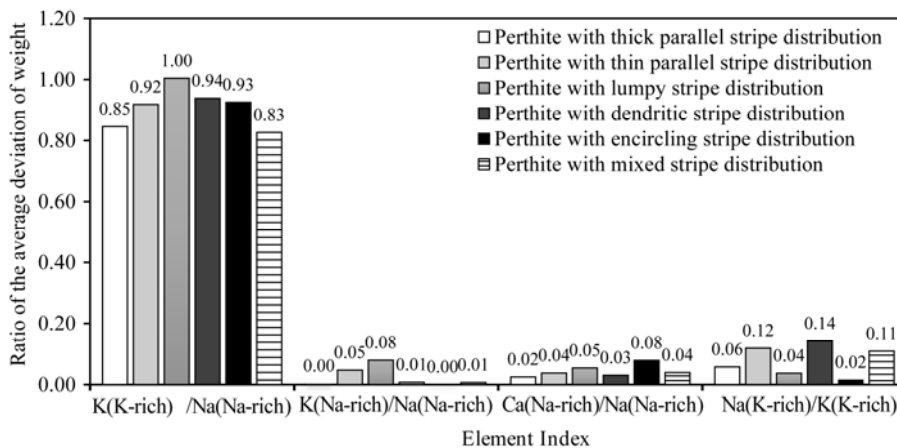


Fig. 10. Ratio of the average deviation of weight in the perthite in tight sandstone.

Table 7 EDS analysis results of perthite with mixed stripe distribution

Sample	Percent (%)	Na-rich feldspar							K-rich feldspar						
		C	Na	Al	Si	Ca	O	K	C	Na	Al	Si	K	O	Ba
1	Weight	2.58	6.96	9.61	28.71	1.13	51.01		3.04		8.36	27.90	11.12	49.58	
	Atomic	4.20	5.92	6.97	20.00	0.55	62.36		5.12		6.28	20.11	5.76	62.74	
2	Weight	3.06	7.40	8.85	29.02		51.67		3.17	0.61	8.28	27.69	10.52	49.72	
	Atomic	4.94	6.23	6.34	20.00		62.50		5.32	0.54	6.19	19.88	5.42	62.65	
3	Weight	2.68	7.81	8.95	29.33		51.23		2.87	0.79	8.59	28.06	10.11	49.59	
	Atomic	4.33	6.60	6.46	20.32		62.29		4.83	0.69	6.43	20.19	5.23	62.64	
4	Weight	2.07	7.75	9.58	29.41	0.68	50.51		2.40		8.70	28.62	11.27	49.03	
	Atomic	3.39	6.63	6.98	20.59	0.33	62.08		4.08		6.59	20.82	5.89	62.62	
5	Weight	1.80	8.31	9.24	30.28		50.38			0.63	9.43	31.27	11.98	46.69	
	Atomic	2.94	7.11	6.74	21.22		61.99			0.58	7.41	23.62	6.50	61.89	
6	Weight	3.67	7.56	8.48	28.21		52.09		4.05	0.35	8.28	26.37	10.49	50.47	
	Atomic	5.87	6.31	6.03	19.28		62.51		6.72	0.30	6.11	18.70	5.34	62.83	
7	Weight	3.39	7.83	8.44	28.56		51.79		4.59	1.12	7.80	26.10	9.19	51.19	
	Atomic	5.43	6.57	6.03	19.60		62.38		7.52	0.96	5.69	18.28	4.62	62.93	
8	Weight	4.22	6.77	9.17	26.52	0.97	52.35		4.68	1.46	7.98	25.76	8.89	51.23	
	Atomic	6.73	5.64	6.50	18.06	0.46	62.61		7.64	1.24	5.81	18.00	4.46	62.85	
9	Weight	1.63	7.37	10.63	28.61	2.01	49.75		6.49	1.22	7.52	22.97	7.53	52.33	1.94
	Atomic	2.70	6.38	7.83	20.25	1.00	61.84		10.45	1.03	5.39	15.83	3.73	63.30	0.27
10	Weight	3.75	7.34	8.75	27.58	0.60	51.99		3.40	0.50	8.46	27.38	10.22	50.04	
	Atomic	6.00	6.14	6.24	18.87	0.29	62.46		5.68	0.44	6.30	19.57	5.25	62.78	
11	Weight	5.07	6.84	8.20	25.67	0.48	52.81	0.94	6.69		7.22	23.65	9.34	53.10	
	Atomic	8.00	5.64	5.76	17.33	0.23	62.58	0.45	10.66		5.13	16.12	4.57	63.53	
12	Weight	2.77	7.37	8.80	29.58		51.48		3.00	0.56	8.56	27.67	10.68	49.52	
	Atomic	4.48	6.23	6.34	20.46		62.50		5.06	0.49	6.42	19.92	5.52	62.59	

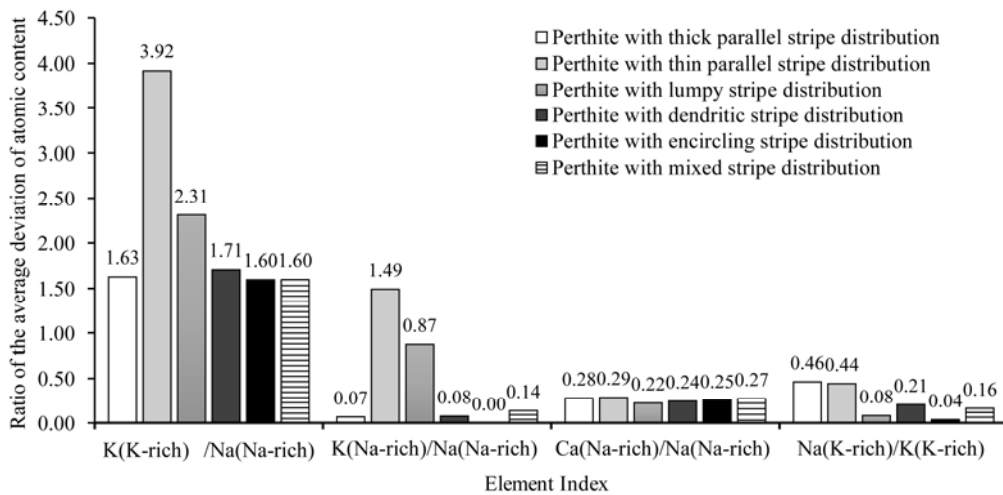


Fig. 11. Ratio of the average deviation of atomic content in the perthite in tight sandstone.

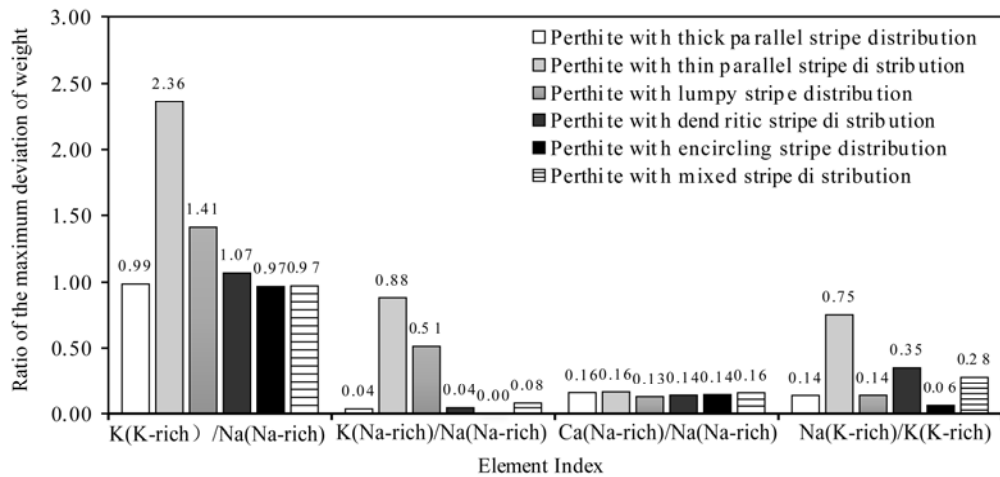


Fig. 12. Ratio of the maximum deviation of weight in the perthite in tight sandstone.

In the above analysis the level sequence of each element index has been determined. Through this analysis, the different perthite types of these indexes have been identified. The identification of some perthite types is better than others. Since the standard deviation of a set of data indicates the degree of dispersion, the higher the standard deviation, the higher the degree of dispersion of the data set, and the more effectively perthite types could be identified.

In the following analysis, the standard deviation of each element index was calculated and used as the evaluation criteria so that the preferred element index to identify the perthite types could be determined.

Table 8 shows that the element indexes such as ‘average-weight-K(K-rich)/Na(Na-rich)’, ‘maximum-weight-K(Na-rich)/Na(Na-rich)’, ‘average-atomic-K(K-rich)/Na(Na-rich)’, etc., can be the most effective to identify perthite types because the standard deviation of the two indicators is the largest, indicating that the two indicators have a greater distinction in judging the morphology of the perthite, so they have good applicability. Similarly, the other indicators shown in Fig. 9 can also be used as judgement indicators. The larger the standard deviation, the less applicable they are. We were able to decide which index to use according to the conditions of practical research.

In other words, the perthite types were easily identified when appropriate element indexes were combined. Additionally, identifying the perthite types also allowed for the discovery of the element distribution of K-rich and Na-rich feldspars in the perthite.

Comparison of the analysis results with the classification results allowed several element indexes to be calculated, and statistics of the occurrence probability of K in Na-rich feldspar, Ca in Na-rich feldspar, and Na in K-rich feldspar were also calculated to identify different shapes of perthite. From these statistics, the distribution of elements through the perthite shapes was predicted. Therefore, the study provided a scientific basis for the discovery of the formation mechanism of the minerals in the Yanchang Formation tight sandstone.

5 Conclusions

The large amount of feldspar in tight sandstone was able

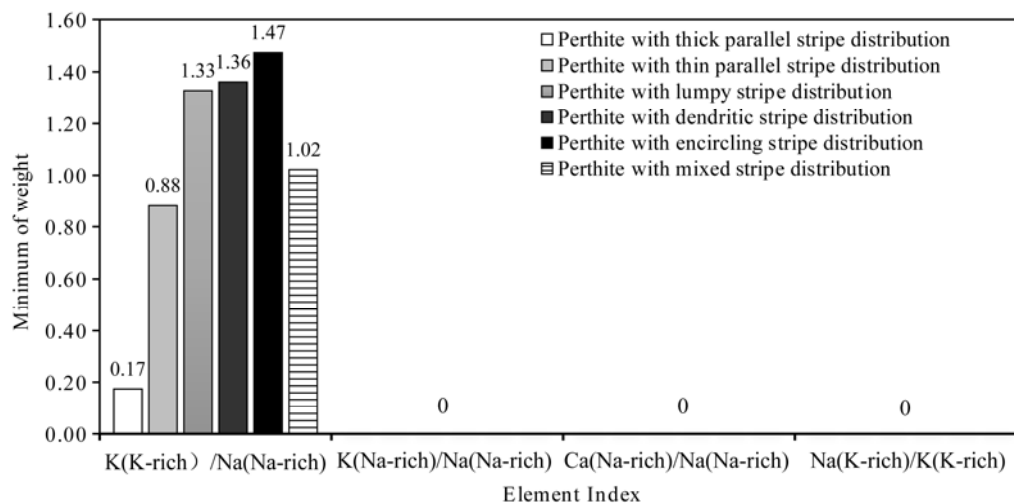


Fig. 13. Ratio of the maximum deviation of atomic content in the perthite in tight sandstone.

Table 8 Standard deviation of the element indexes in six types of perthite

Rank	Element index	Standard deviation
1	Average-weight-K(K-rich) /Na(Na-rich)	0.839
2	Maximum-weight-K(Na-rich)/Na(Na-rich)	0.555
3	Average-atomic-K (K-rich) /Na(Na-rich)	0.502
4	Average-weight-K(K-rich) /Na(Na-rich)	0.437
5	Maximum-atomic-K(Na-rich)/Na(Na-rich)	0.328
6	Average-weight-K(K-rich) /Na(Na-rich)	0.232
7	Standard deviation-atomic-Na(K-rich)/K(K-rich)	0.229
8	Probability of the occurrence of "Na" in K-rich feldspar	0.211
9	Average-weight-K(K-rich) /Na(Na-rich)	0.199
10	Probability of the occurrence of "Ca" in Na-rich feldspar	0.188
11	Standard deviation-weight-Na(K-rich)/K(K-rich)	0.165
12	Average-atomic-K (K-rich) /Na(Na-rich)	0.137
13	Maximum-weight-K(Na-rich)/Na(Na-rich)	0.124
14	Average-atomic-K (K-rich) /Na(Na-rich)	0.089
15	Maximum-atomic-K(Na-rich)/Na(Na-rich)	0.073
16	Probability of the occurrence of "KandNa-rich feldspar	0.065
17	Average-atomic-K (K-rich) /Na(Na-rich)	0.059
18	Maximum-weight-K(Na-rich)/Na(Na-rich)	0.050
19	Standard deviation-weight-Na(K-rich)/K(K-rich)	0.047
20	Standard deviation-atomic-Na(K-rich)/K(K-rich)	0.046
21	Standard deviation-atomic-Na(K-rich)/K(K-rich)	0.046
22	Standard deviation-weight-Na(K-rich)/K(K-rich)	0.039
23	Minimum-weight-Ca(Na-rich)/Na(Na-rich)	0.032
24	Maximum-atomic-K(Na-rich)/Na(Na-rich)	0.029
25	Minimum-weight-Ca(Na-rich)/Na(Na-rich)	0.022
26	Minimum-atomic-Ca(Na-rich)/Na(Na-rich)	0.018
27	Minimum-atomic-Ca(Na-rich)/Na(Na-rich)	0.012
28	Minimum-weight-Ca(Na-rich)/Na(Na-rich)	0.008
29	Minimum-atomic-Ca(Na-rich)/Na(Na-rich)	0.004
30	Maximum-weight-K(Na-rich)/Na(Na-rich)	0
31	Minimum-weight-Ca(Na-rich)/Na(Na-rich)	0
32	Standard deviation-Weight-Na(K-rich)/K(K-rich)	0
33	Maximum-atomic-K(Na-rich)/Na(Na-rich)	0
34	Minimum-atomic-Ca(Na-rich)/Na(Na-rich)	0
35	Standard deviation-atomic-Na(K-rich)/K(K-rich)	0

to provide the material basis for the formation of perthite. Significant differences exist in the morphology of Na-rich feldspar when we treat K-rich feldspar as the main component of perthite. The perthite in tight sandstone from the Ordos basin has been divided into six main types based on morphological characteristics, which are perthite with thick parallel stripe distribution; with thin parallel stripe distribution; with lumpy stripe distribution; with dendritic stripe distribution; with encircling stripe

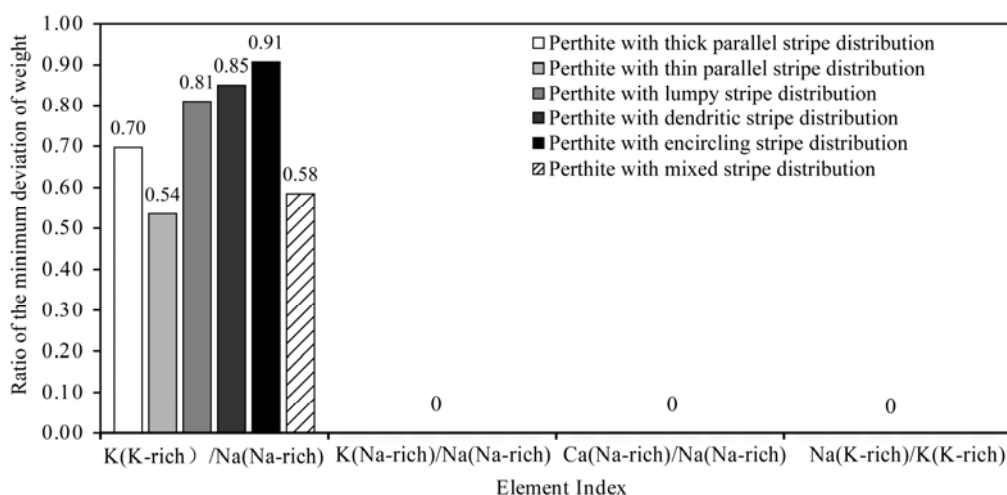


Fig. 14. Ratio of the minimum deviation of weight in the perthite in tight sandstone.

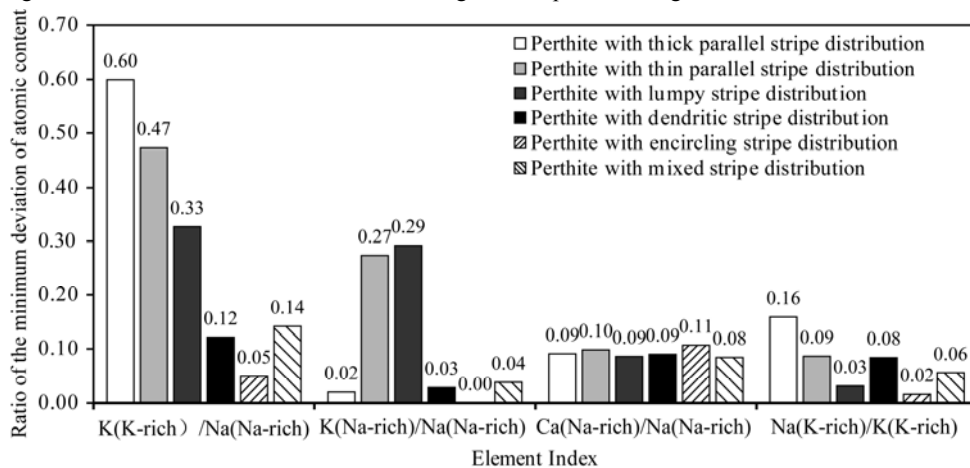


Fig. 15. Ratio of the minimum deviation of atomic content in the perthite in tight sandstone.

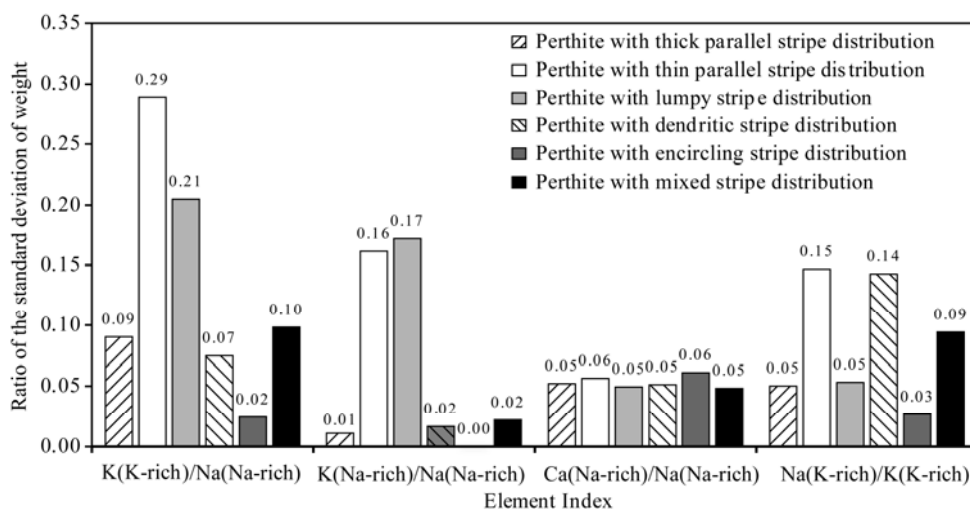


Fig. 16. Ratio of the standard deviation of weight in the perthite in tight sandstone.

distribution; and with mixed stripe distribution.

These different types of perthite have clear differences in the different element indexes.

Element indexes such as average-weight-K (K-rich) / Na (Na-rich), maximum-weight-K (Na-rich) / Na (Na-rich), average-atomic-K (K-rich) / Na (Na-rich), etc., are

probably or possibly the most effective ones to use for identifying the types of perthite. The perthite types can then be easily identified combining the appropriate element indexes. Additionally, identification of the perthite types has allowed for the discovery of the distribution of elements of K-rich and Na-rich feldspar in perthite.

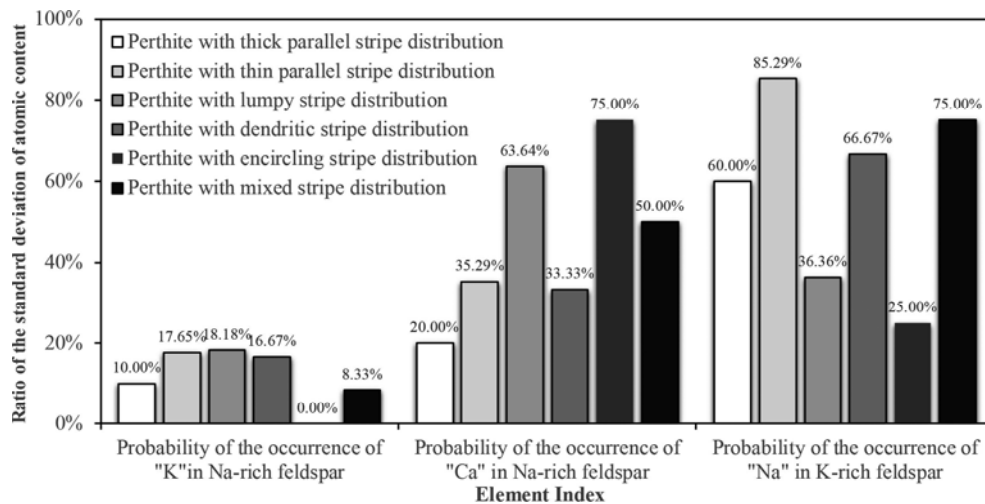


Fig. 17. Ratio of the standard deviation of atomic content in the perthite in tight sandstone.

Acknowledgements

This work was funded by open fund of Key Laboratory of Petroleum Resources Research, Institute of Geology and Geophysics, Chinese Academy of Sciences (grant No. KLOR2018-6) and the National Science and Technology Project of China (grant No. 2017ZX05013005-009). Thanks are given to Gao Xiaoli, Jin Xiangtian and Chai Guangsheng for their help in this study.

Manuscript received Aug. 11, 2018
 accepted Oct. 27, 2018
 associate EIC HAO Ziguang
 edited by HAO Qingqing

References

- Alexandre, P., 2009. Mineralogy and geochemistry of the sodium metasomatism-related uranium occurrence of Aricheng South, Guyana. *Mineralium Deposita*, 45: 351–367.
- Ao Weihua, Huang Wenhui, Weng Chengmin, Xiao Xiuling, Liu Dameng, Tang Xiuyi, Chen Ping, Zhao Zhigen, Wan Huan and Robert B Finkelman, 2012. Coal petrology and genesis of Jurassic coal in the Ordos Basin, China. *Geoscience Frontiers*, 3(1): 85–95.
- Connors, K.A., and Page, R.W., 1995. Relationship between magmatism, metamorphism and deformation in the western Mount Isa Inlier, Australia. *Precambrian Research*, 71: 131–153.
- Cuney, M., Emetz, A., Mercadier, J., Mykchaylov, V., Shunko, V., and Yuslenko, A., 2013. Uranium deposits associated with Na-metasomatism from central Ukraine: a review of some of the major deposits and genetic constraints. *Ore Geology Reviews*, 44: 82–106.
- Dai, S., Liu, J., Ward, C.R., Hower, J.C., Xie, P., and Jiang, Y., 2015. Petrological, geochemical, and mineralogical compositions of the low-Ge coals from the Shengli Coalfield, China: a comparative study with Ge-rich coals and a formation model for coal-hosted Ge ore deposit. *Ore Geology Reviews*, 71: 318–349.
- Ding, T., 1994. Altered volcanic-ash layers in coal-bearing sequences. *Geochimica et Cosmochimica Acta*, 58: 1–44.
- Eurico Zimbres, 2006. *An antiperthitic intergrowth of K-feldspar (the veinlets) in the Na-feldspar*. Wikimedia Website. https://commons.wikimedia.org/wiki/File:Antiperthitic_feldspar.jpg.
- Gao Gang, Zhang Weiwei, Ma Guofu, Chen Guo, Li Tao, Hu Lingzhi, Yang Zhiming, Wang Jianguo and Yang Jun, 2018. Mineral composition and organic geochemistry of the Lower Cretaceous Xiagou Formation source rock from the Qingxi Sag, Jiuquan Basin, northwest China. *Petroleum Science*, 15(1): 51–67.
- Huang, X., and Zhao, Y., 2017. Characterization of pore structure, gas adsorption, and spontaneous imbibition in shale gas reservoirs. *Journal of Petroleum Science and Engineering*, 159: 197–204.
- Jarvie, D.M., Hill, R.J., Ruble, T.E., and Pollastro, R.M., 2007. Unconventional shale-gas system: the Mississippian Barnett shale on north-center Texas as one model for thermogenic shale-gas assessment. *AAPG Bulletin*, 91: 475–499.
- Kuschke, O., and Tonking, M., 1971. Geology and mining operations at Palabora Mining Company Ltd, Phalaborwa, NE Transvaal. *Journal of the South African Institute of Mining & Metallurgy*, 72: 12–22.
- Lawrence H. Tanner, Wang Xin and Alesha C Morabito, 2012. Fossil charcoal from the Middle Jurassic of the Ordos Basin, China and its paleoatmospheric implications. *Geoscience Frontiers*, 3(4): 493–502.
- Liao Jianbo, Xi Aihua, Li Zhiyong, Liu Huaqing, Li Xiangbo and Wanyan Rong, 2018. Microscopic characterization and formation mechanisms of deep-water sandy-debris-flow and turbidity-current sandstones in a lacustrine basin: a case study in the Yanchang Formation of the Ordos Basin, China. *Petroleum Science*, 15(1): 28–40.
- Ma Hongwen, Yang Jing, Su Shuangqing and Yao Wengui, 2017. Compositions, proportions, and equilibrium temperature of coexisting two-feldspar in crystalline rocks. *Acta Geologica Sinica (English Edition)*, 91(3): 875–881.
- Macquaker, J.H.S., Taylor, K.G., Keller, M., and Polya, D., 2014. Compositional controls on early diagenetic pathways in fine-grained sedimentary rocks: implications for predicting unconventional reservoir attributes of mudstones. *AAPG Bulletin*, 93: 587–603.
- Mezni, M., Hamzaoui, A., Hamdi, N., and Srasra, E., 2011. Synthesis of zeolites from the low-grade Tunisian natural illite by two different methods. *Applied Clay Science*, 52: 209–218.
- Montgomery, S.L., Jarvie, D.M., Bowker, K.A., and Pollastro, R.M., 2005. Mississippian Barnett shale, Fort Worth Basin, North-Central Texas: gas-shale play with multi-trillion cubic foot potential. *AAPG Bulletin*, 89: 155–175.
- Novembre, D., Sabatino, B.D., and Gimeno, D., 2005. Synthesis of Na-A zeolite from 10 Å halloysite and a new crystallization kinetic model for the transformation of Na-A into HS zeolite. *Clays and Clay Minerals*, 53: 28–36.
- Salem, A.M., Ketzer, J.M., Morad, S., Rizk, R.R., and Al-Aasm, I.S., 2005. Diagenesis and reservoir-quality evolution of incised-valley sandstones: evidence from the Abu Madi gas reservoirs (upper Miocene), the Nile Delta basin, Egypt. *Journal of Sedimentary Research*, 75: 572–584.

- Sheng Jun, Xu Li, Wang Qi, Yang Cheng, DingXiaoJun and Liu Yanni, 2018. The seepage characteristics of different pore types of tight sandstone gas reservoir—taking the southeast area of Sulige gas field, Ordos Basin as an example. *Geological Review*, 64(3): 764–776 (in Chinese with English abstract).
- Sun Jiaopeng and Dong Yunpeng, 2019. Middle-Late Triassic sedimentation in the Helanshan tectonic belt: constraint on the tectono-sedimentary evolution of the Ordos Basin, North China. *Geoscience Frontiers*, 10: 213–227.
- Tan Juanjuan, Mei Yuping, Yang Hongmei, Lu Shansong, Duan Ruichun and Qiu Xiaofei, 2017. Ar-Ar geochronology study on K-feldspar in Xishan W-Sn ore deposit in Yangchun, Guangdong Province. *Acta Geologica Sinica (English Edition)*, 91(z1):189–190.
- Tang Xuan, Zhang Jinchuan, Shan Yansheng and Xiong Jinyu, 2012. Upper Paleozoic coal measures and unconventional natural gas systems of the Ordos Basin, China. *Geoscience Frontiers*, 3(6): 863–873.
- Vengosha, A., Warnera, N., Jacksona, R., and Darraha, T., 2013. The effects of shale gas exploration and hydraulic fracturing on the quality of water resources in the United States. *Procedia Earth and Planetary Science*, 7: 863–866.
- Wang Zhentao, Zhou Hongrui, Wang Xunlian and Jing Xiuchun, 2015. Characteristics of the crystalline basement beneath the Ordos Basin: constraint from aeromagnetic data. *Geoscience Frontiers*, 6(3): 465–475.
- Wang, H., Feng, Q., Liu, K., Li, Z., and Tang, X., 2017. Highly efficient fluoride adsorption from aqueous solution by nepheline prepared from kaolinite through alkali-hydrothermal process. *Journal of Environmental Management*, 196: 72–79.
- Wilde, A.R., 2011. Mount Isa copper orebodies: improving predictive discovery. *Australian Journal of Earth Sciences*, 58: 937–951.
- Wilde, A.R., 2013. Towards a model for albitite-type uranium. *Minerals*, 3: 36–48.
- Wu, X., Zhou, T., Chen, Y., Zhang, Z., Piao, G., and Kobayashi, N., 2011. Mineral melting behavior of Chinese blended coal ash under gasification condition. *Asia-Pacific Journal of Chemical Engineering*, 6: 220–230.
- Xin, G., Cole, D.R., Rother, G., Mildner, D.F.R., and Brantley, S.L., 2015. Pores in Marcellus shale: a neutron scattering and FIB-SEM study. *Energy Fuels*, 29: 1295–1308.
- Xue Chunji, Chi Guoxiang and Xue Wei, 2011. Effects of hydrocarbon generation on fluid flow in the Ordos Basin and its relationship to uranium mineralization. *Geoscience Frontiers*, 2(3): 439–447.
- Zou, C., Zhu, R., Liu, K., Su, L. Bai, B., Zhang, X., Yuan, X., and Wang, J., 2012. Tight gas sandstone reservoirs in China: characteristics and recognition criteria. *Journal of Petroleum Science and Engineering*, 88: 82–91.

About the first author



DU Shuheng, male, born in Anhui in 1994, received his doctoral degree from Peking University and is now an assistant professor at State Key Laboratory of Nonlinear Mechanics, Institute of Mechanics, Chinese Academy of Sciences. His main research interests include the accurate characterization of unconventional oil and gas reservoirs, and key mechanical problems in unconventional oil and gas exploitation.

Address: No. 15, North Fourth Ring Road West, Haidian District, Beijing, 100190. E-mail: dushuheng@imech.ac.cn.